Harmonics of Outer Hair Cell Motility

J. Santos-Sacchi
Sections of Otolaryngology and Neurobiology, Yale University School of Medicine, New Haven, Connecticut 06510 USA

ABSTRACT The voltage-dependent mechanical activity of outer hair cells (OHC) from the organ of Corti is considered responsible for the peripheral auditory system's enhanced ability to detect and analyze sound. Nonlinear processes within the inner ear are presumed to be characteristic of this enhancement process. Harmonic distortion in the OHC mechanical response was analyzed under whole-cell voltage clamp. It is shown that the OHC produces DC, fundamental and second harmonic length changes in response to sinusoidal transmembrane voltage stimulation. Mechanical second harmonic distortion decreases with frequency, whereas the predicted transmembrane second harmonic voltage increases with frequency. Furthermore, the phase of the second harmonic distortion does not correspond to the phase of the predicted transmembrane voltage. In contradistinction, it has been previously shown (Santos-Sacchi, J. 1992. *Neuroscience.* 12:1906–1916) that fundamental voltage and evoked mechanical responses share magnitude and phase characteristics. OHC length changes are modeled as resulting from voltage-dependent cell surface area changes. The model suggests that the observed harmonic responses in the mechanical response are consistent with the nonlinearity of the voltage-to-length change (V-δL) function. While these conclusions hold for the data obtained with the present voltage clamp protocol and help to understand the mechanism of OHC motility, modeling the electromechanical system of the OHC in the in vivo state indicates that the mechanical nonlinearity of the OHC contributes minimally to mechanical distortion. That is, in vivo, at moderate sound pressure levels and below, the dominant factor which contributes to nonlinearities of the OHC mechanical response resides within the nonlinear, voltage-generating, stereociliar transduction process.

INTRODUCTION

The organ of Corti, the mammalian auditory sensory epithelium, possesses two types of sensory cells, the inner (IHC) and outer (OHC) hair cells. The OHC has received a tremendous amount of attention in the last decade, primarily because it appears to function as both receptor and effector (Brownell, 1992; Dallos, 1992). The OHC produces receptor potentials in response to acoustic stimulation (Dallos et al., 1982; Russell et al., 1986), and rapidly alters its length as a function of transmembrane voltage (Ashmore, 1987; Santos-Sacchi and Dilger, 1988; Santos-Sacchi, 1992). Currently, the OHC is presumed to modify basilar membrane motion through a mechanical feedback mechanism (Ruggero, 1992). This feedback is ultimately considered to enhance the tuning and sensitivity characteristics of the inner hair cell, the cell type which is innervated by the majority of eighth nerve fibers.

Factors which influence the voltages generated in the OHC are therefore crucial in understanding the impact of the postulated OHC mechanical feedback within the organ of Corti. There are a variety of intrinsic nonlinear processes which may shape the voltages controlling OHC mechanical activity. Included are asymmetrical transduction processes (Russell et al., 1986; Dallos, 1986), and voltage-dependent basolateral membrane conductances (Santos-Sacchi and Dilger, 1988; Ashmore and Meech, 1986; Nakagawa et al., 1991; Housley and Ashmore, 1992) and capacitance (Ashmore, 1989; Santos-Sacchi, 1990, 1991). These nonlinearities will be expected to generate distortions (DC and harmonic components) in AC membrane voltages, which should be reflected in the voltage-dependent mechanical activity of the OHC. In this report, I evaluate the OHC mechanical response with the whole cell voltage clamp, under conditions where the nonlinear basolateral and transducer conductances contribute minimally. It is demonstrated that fundamental and harmonic mechanical responses are generated upon sinusoidal transmembrane voltage stimulation. Furthermore, it is shown that the phase of the second mechanical harmonic does not correspond to the phase of the second voltage harmonic. Thus, while the phase and magnitude of the fundamental mechanical component mirror that of the fundamental membrane voltage (Santos-Sacchi, 1992), the nonlinearity of the voltage-to-length change (V-δL) function dominates the production of higher mechanical harmonics under voltage clamp at the voltage magnitudes studied. Nevertheless, through modeling, it is shown that mechanical nonlinearities in the in vivo situation will be a dominant function of voltage nonlinearities effected by the stereociliar transducer mechanism.

MATERIALS AND METHODS

General

Guinea pigs were overdosed with pentobarbital. The temporal bones were removed, and OHCs were isolated nonenzymatically from the cochleas by gentle pipetting of the isolated top two turns of the organ of Corti in Ca^{2+}-free medium. OHC stereocilia are damaged or lost during this treatment. The cell-enriched supernatant was then transferred to a 700-ml perfusion chamber, and the cells permitted to settle onto the cover glass bottom. All experiments were performed at room temperature (~23°C). A Nikon Diaphot inverted microscope with Hoffmann optics was used to observe the cells during electrical and mechanical recording. All experiments were taped with

Received for publication 29 March 1993 and in final form 25 June 1993.
Address reprint requests to Joseph Santos-Sacchi.

0006-3495/93/11/2217/11 $2.00

a Panasonic AG6300 video recorder. A modified Leibovitz medium (142.2 mM NaCl, 5.37 mM KCl, 1.25 mM $CaCl_2$, 1.48 mM $MgCl_2$, 5.0 mM 4-(2-hydroxyethyl)-1-piperazineethanesulfonic acid, 5.0 mM dextrose, pH 7.2) was used as the normal perfusate. Modifications made to the extracellular medium in order to block ionic conductances are noted in figure legends. NaCl was adjusted to maintain osmolarity (300 mOsm).

Electrical recording

OHCs were whole cell voltage-clamped with a Dagan patch clamp amplifier at holding potentials between −70 and −80 mV, similar to potentials recorded in vivo (Dallos et al., 1982). Pipette solutions were composed of 140 mM CsCl, 5 or 10 mM EGTA, 2 mM $MgCl_2$, and 5 mM 4-(2-hydroxyethyl)-1-piperazineethanesulfonic acid buffered to pH 7.2. Gigohm seals were obtained at the nuclear level of the cell membrane and electrode capacitance was compensated prior to whole cell recording. AC studies were performed using a digital signal-processing board with custom written software (DSP-16; Ariel Corp., Highland Park, NJ), capable of delivering and analyzing pure tone or swept frequency stimuli. Data were saved to disk for off-line analysis.

Electrode resistance (R_s), membrane resistance (R_m), and capacitance (C_m) were estimated from current transients evoked by small voltage steps (Santos-Sacchi, 1992). Care was taken to maintain low series resistance values during recording by delivering transient positive or negative pressure into the electrode to maintain an unobstructed orifice; electronic series resistance compensation was employed as well. Measurements were made on a physical R-C cell model to rule out potential artifacts generated within the voltage clamp system.

OHC Motility Measures

OHC mechanical responses and currents were simultaneously measured in response to sinusoidal voltage stimuli. Fast OHC movements were measured with a differential photodiode (PD) onto which the image of the cuticular plate (apical end of cell) from the microscope was projected (Santos-Sacchi, 1992). Placement of the PD was accomplished remotely by a computer-controlled micromanipulator, so as not to perturb whole cell recording. The frequency response of the PD system, measured with an LED, had a 3-dB rolloff at 6 kHz. Sinusoidal voltage bursts (onset and offset linearly ramped) were delivered to OHCs under voltage clamp. PD output and whole cell currents were filtered at 10 kHz (12 dB/octave) and collected simultaneously using a sampling rate of 20 kHz. Responses were averaged 200 times. Magnitude and phase of the current and mechanical responses were measured by fast Fourier transform of the central portion of the digitized waveforms using the software package Matlab (Mathworks, Natick, MA). Numerical solutions to model equations were also performed with this package. Mechanical responses were corrected for the phase and magnitude characteristics of the PD system. The pertinent response characteristics of the system were evaluated by measuring the movements of a glass probe driven by a piezoelectric bimorph (Fig.1). Since the measured quantities in these experiments are the change in cell length (δL) and the current through the resistance of the patch electrode (I_{R_s}), all phase relations (data and model) are conveniently referenced to that of current (I_{R_s}). That is, fundamental movement phase [$\phi(\delta L_{fo})$] is referenced to fundamental current phase [$\phi(I_{Rsfo})$], and harmonic movement phase [$\phi(\delta L_{fn})$] is referenced to harmonic current phase [$\phi(I_{Rsfn})$]. Absolute calibration of cell movements was determined by measuring off the video monitor the cell movement in response to a large steady state depolarizing voltage stimulus (Santos-Sacchi, 1989).

RESULTS

Sinusoidal voltage stimulation of the OHC produces sinusoidal alterations in the cell's length. Fig. 2 illustrates, for three cells, the waveforms, magnitudes, and phases of the

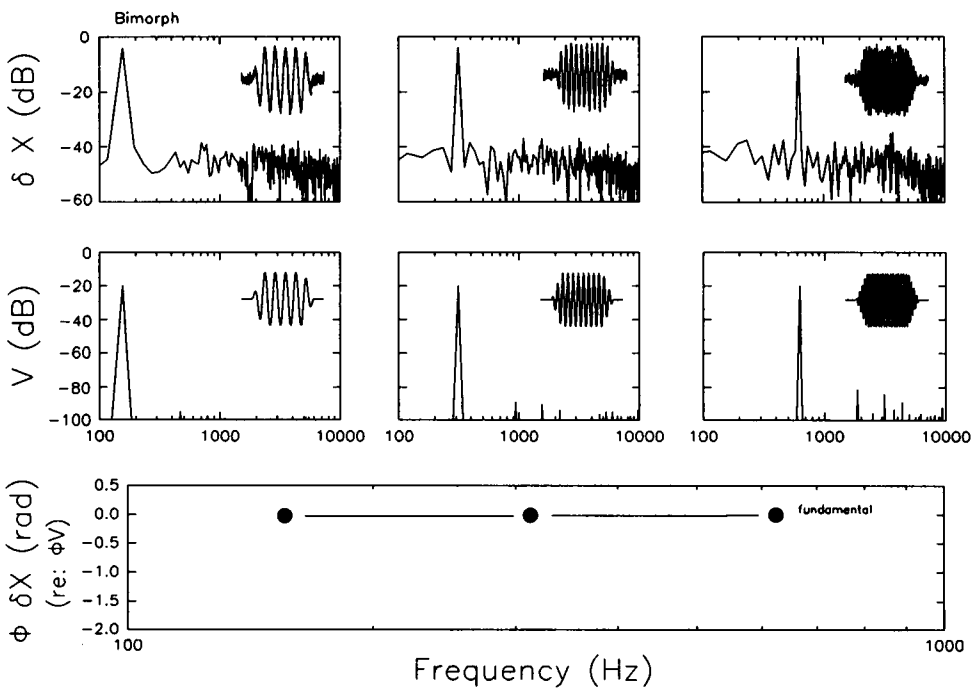

FIGURE 1 Characteristics of the mechanical measurement system. Outputs from PD in response to simulated cell movement. The tip of a glass microelectrode shank was melted to a sphere of about 15 μm; transmitted light produced a bright area in the sphere's center which was used to mimic the bright OHC cuticular plate observed under Hoffmann optics. The artificial cell was attached to a piezoelectric bimorph and moved using the same voltage waveforms that were used to collect OHC movement data. Upper panel depicts the movement waveforms and magnitude responses obtained by FFT for the stimulus frequencies of 156, 313, and 625 Hz. Peak to peak movements were about 1 μm. Middle panel depicts the voltage stimulus waveforms and magnitude responses. Note that only fundamental components are observed, indicating the linearity of the measurement system. Lower panel shows the phase of the mechanical response fundamental relative to the driving voltage. As expected for the voltage-dependent piezoelectric response, the phase difference is zero.

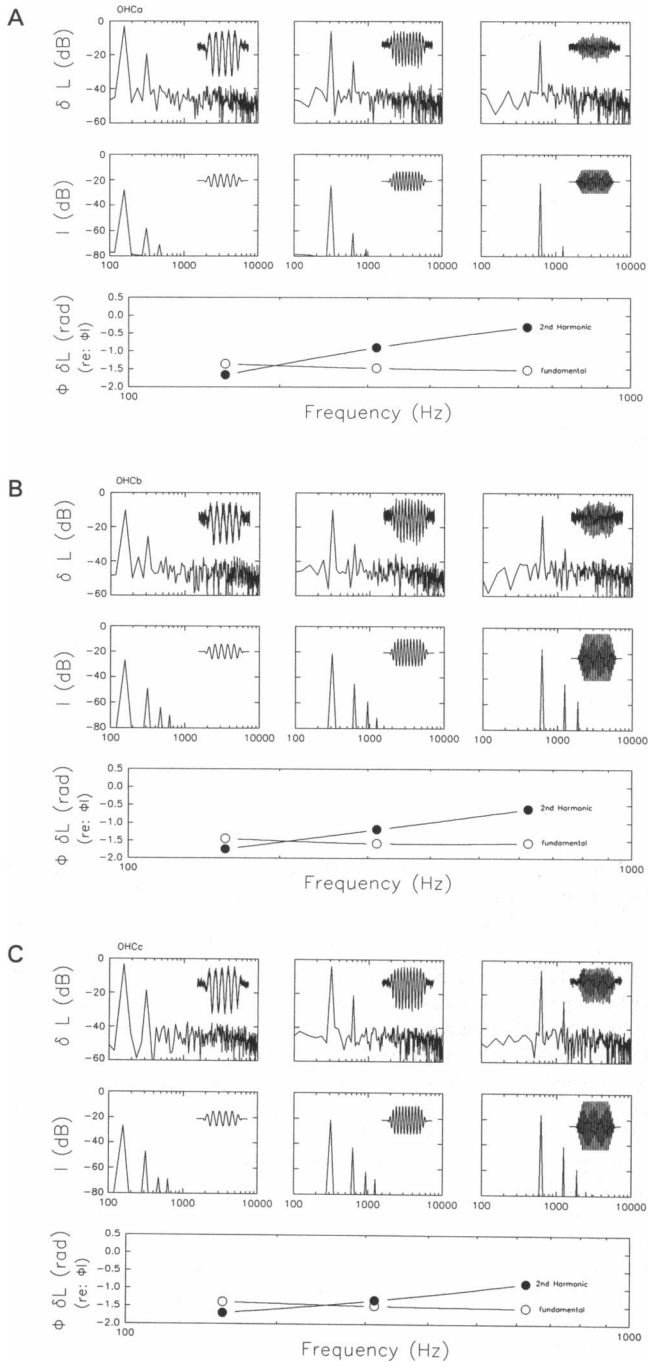

FIGURE 2 OHC mechanical responses induced by sinusoidal voltage clamp stimulation. Results from three different cells are presented in *A*, *B*, and *C*. Upper panels depict the movement waveforms and magnitude responses obtained by FFT for the stimulus frequencies of 156, 313, and 625 Hz. Middle panels depict the measured current waveforms and magnitude responses. Peak-to-peak movements at low frequency were about 1 μm. Lower panel shows the phase of the mechanical response fundamental and second harmonic relative to the measured current phase. Phase is plotted versus fundamental frequency. Note in each case that the mechanical response consists of a DC, fundamental, and second harmonic response. The phase of the fundamental mechanical component asymptotes near −1.57 rad, while that of the second harmonic presents an initial phase lag of greater than −1.57 rad which decreases as frequency increases. Clamp-cell electrical characteristics: (*A*) R_m = 96 MΩ; C_m = 24.73 pF; clamp tau = 0.553 ms. Nominal peak voltage was 60 mV. CsCl electrode. Extracellular medium was Leibovitz with 20 mM TEA. (*B*) R_m = 79 MΩ; C_m = 41.89 pF; clamp tau = 0.128 ms. Nominal peak voltage was 40 mV. CsCl electrode. Extracellular medium was Leibovitz with 20 mM TEA, 300 nM TTX, and 1 mM $CdCl_2$. (*C*) Nominal peak voltage: 50 mV. CsCl electrode. Extracellular medium was Ca^{2+}-free Leibovitz with 20 mM TEA and 20 mM CsCl. R_m = 125 MΩ; C_m = 35.4 pF; and clamp tau = 0.125 ms.

measured mechanical and current responses at three frequencies, 156, 313, and 625 Hz. In addition to the fundamental component, the mechanical responses exhibit nonlinear characteristics, including a DC component and a second harmonic (higher harmonics may lie below the noise floor). In all cells successfully recorded from (n = 9), harmonics were observed. The DC component is clearly due to the nonlinear form of the V-δL function, and the position of the holding potential along this function (Santos-Sacchi, 1989; Evans et al., 1989). The phase of the mechanical fundamental relative to the current fundamental differs by some 1.5 rad at these frequencies; this has been observed to be characteristic of a voltage-driven mechanical process (Santos-Sacchi, 1992). Note, however, that the phase of the mechanical second harmonic relative to the current second harmonic demonstrates a phase lag which decreases as frequency increases. This, as will be demonstrated below, is not characteristic of a directly driven voltage-induced mechanical response.

As a first step toward evaluating the data, the OHC is modeled to determine the currents and voltages generated under whole cell voltage clamp. The electrical characteristics of the OHC when ionic conductances are blocked can be modeled most simply as an electrode resistance (access resistance, R_s) in series with a parallel combination of a membrane resistance (R_m), a linear membrane capacitance (C_{lin}), and a voltage-dependent membrane capacitance (C_v) (Fig. 3 *a*).[1] The total membrane capacitance (C_m) at any given voltage is the sum of the linear and nonlinear capacitances,

$$C_m = C_v + C_{lin}, \tag{1}$$

where C_v is defined as the first derivative of the Boltzmann function relating OHC nonlinear charge movement and voltage (see Santos-Sacchi, 1991). Thus,

$$C_v = \frac{(Q_{max}(ze/kT))}{\exp\left(\frac{ze}{kT}\{V_m - V_h\}\right)\left[1 + \exp\left(\frac{-ze}{kT}\{V_m - V_h\}\right)\right]^2}, \tag{2}$$

where V_m is the membrane potential, V_h is voltage at half-maximal nonlinear charge transfer, e is electron charge, k is Boltzmann's constant, T is absolute temperature, z is the valence, and Q_{max} is maximum charge transfer.

[1] A residual resistive nonlinearity remains in OHCs despite considerable attempts to block ionic conductances (Santos-Sacchi, 1991). However, while this nonlinearity varies markedly in magnitude (essentially absent in some cells), the nonlinear capacitance is robust. Modeling the OHC with a resistive nonlinearity indicates that the capacitive nonlinearity dominates. Thus, any residual resistive nonlinearity is ignored in the model.

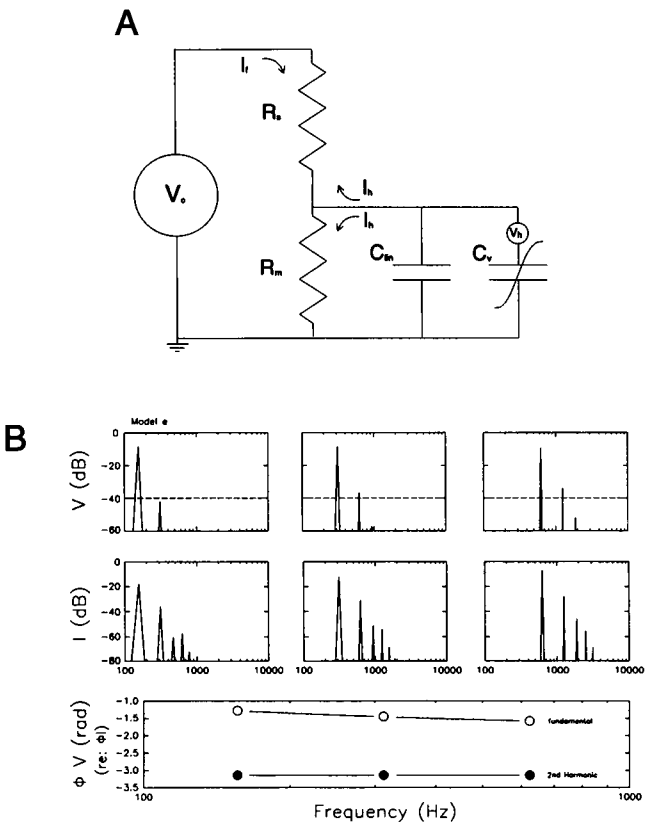

FIGURE 3 (*A*) OHC-clamp model used to determine the currents and voltages generated under whole cell voltage clamp. The model consists of an electrode resistance (access resistance, R_s) in series with a parallel combination of a membrane resistance (R_m), a linear membrane capacitance (C_{lin}), and a voltage-dependent membrane capacitance (C_v). V_c is the voltage clamp source and V_h is the source of the harmonic voltages within the voltage-dependent capacitance. I_f denotes the direction of fundamental currents through R_s elicited by the voltage clamp source. I_h denotes the direction of harmonic currents through R_s and R_m. (*B*) Solution of the model utilizing the parameter value (see Results): V_h, −30 mV; z, −1; Q_{max}, 2 pC; R_m, 100 MΩ; R_s, 5 MΩ; C_{lin}, 20 pF; T, 298K; V_{hold}, −80 mV; and V_c, 40 mV Pk. Upper panel depicts the membrane voltage (V_m) magnitude responses obtained by FFT for the stimulus frequencies of 156, 313, and 625 Hz. Middle panel depicts the current (I_{R_s}) magnitude responses. Note that fundamental and harmonic components are observed, as is expected in a nonlinear system under nonideal voltage clamp. Lower panel shows the phase of the voltage response fundamental relative to the driving current. As expected the phase of the fundamental voltage asymptotes near −1.57 rad, and the phase of the second harmonic voltage is 180° out of phase (−3.12 rad) with the phase of I_{R_s}.

Given an AC command voltage of V_c which is offset by a holding potential of V_{hold}, the current measurable under whole cell voltage clamp, I_{R_s}, is given as

$$I_{R_s} = I_{R_m} + I_{C_m} \tag{3}$$

or

$$\frac{([V_c + V_{hold}] - V_m)}{R_s} = \frac{V_m}{R_m} + C_m \frac{\delta V_m}{\delta t}. \tag{4}$$

Numerical solutions were obtained with typical empirically determined parameter values (Santos-Sacchi (1991): V_h, −30 mV; z, −1; Q_{max}, 2 pC; R_m, 100 MΩ; R_s, 5 MΩ; C_{lin}, 20 pF; T, 298K; V_{hold}, −80 mV; and V_c, 40 mV Pk).

Fig. 3 *b* demonstrates, in the nonlinear electrical model of the OHC under voltage clamp, the current (I_{R_s}) and membrane voltage (V_m) responses due to sinusoidal voltage clamp stimulation. The model generates both fundamental and harmonic responses. Under whole cell voltage clamp, sinusoidal stimulation will elicit voltage harmonics across the nonlinear cell membrane since, due to the finite value of the series resistance, R_s, the clamp is less than ideal (if R_s were equal to zero then the voltage across the membrane would be solely the undistorted sinusoidal clamp voltage). As expected at these frequencies with the chosen typical component values, the phase of the fundamental of V_m lags that of I_{R_s} by about 1.57 rad or 90°. Note, however, that the phase of the second harmonic of V_m lags that of I_{R_s} by 3.14 rad. This derives from the fact that the input voltage clamp stimulus contains no harmonics, and the source of the second harmonic is within the voltage-dependent capacitance, C_v. Thus, at the second harmonic, current flows through R_s and R_m to ground. Keeping the current sign convention through R_s constant (see Fig. 3 *a*), it is apparent why the phase of I_{R_s} at the second harmonic is −3.14 rad relative to that of V_m (i.e., current lags voltage by 3.14 rad). Why, then, if OHC motility is voltage-dependent do the phase characteristics of the motility at the second harmonic differ from those of the voltage predicted by the model?

In order to explore this dilemma, an extension of the simple electrical model is generated whereby the voltage change across the OHC membrane is translated to changes in cell length and cell radius. This mechanical component of the model revolves around the assumption that the voltage-dependent charge movement measured in the OHC (Santos-Sacchi, 1991) corresponds to a conformational change induced by the movement of charged moieties within 10-nm particles known to reside within the OHC plasmalemma (Gulley and Reese, 1977; Saito, 1983; Forge, 1991). The conformational change is assumed to alter the surface area occupied by such particles within the membrane (Fig. 4). Kalinec et al. (1992) have observed depolarization-induced reductions in surface area of OHC lateral membrane patches. Given the constraints of constant cell volume (likely because the OHC mechanical frequency response probably extends beyond a 1-kHz cutoff (Santos-Sacchi, 1992)), and a fixed cell architecture, a change in length and radius will ensue following a change in cell surface area.

The diameter (d_p) of the membrane particle when the cell is fully elongate is taken as 10 nm. The particle area within the membrane is then,

$$A_p = \pi\left(\frac{d_p}{2}\right)^2, \tag{5}$$

and the change in diameter (δd_p) due to voltage-dependent conformation change results in a single particle area change of

$$\delta A_p = \pi\left(\frac{d_p + \delta d_p}{2}\right)^2 - \pi\left(\frac{d_p}{2}\right)^2. \tag{6}$$

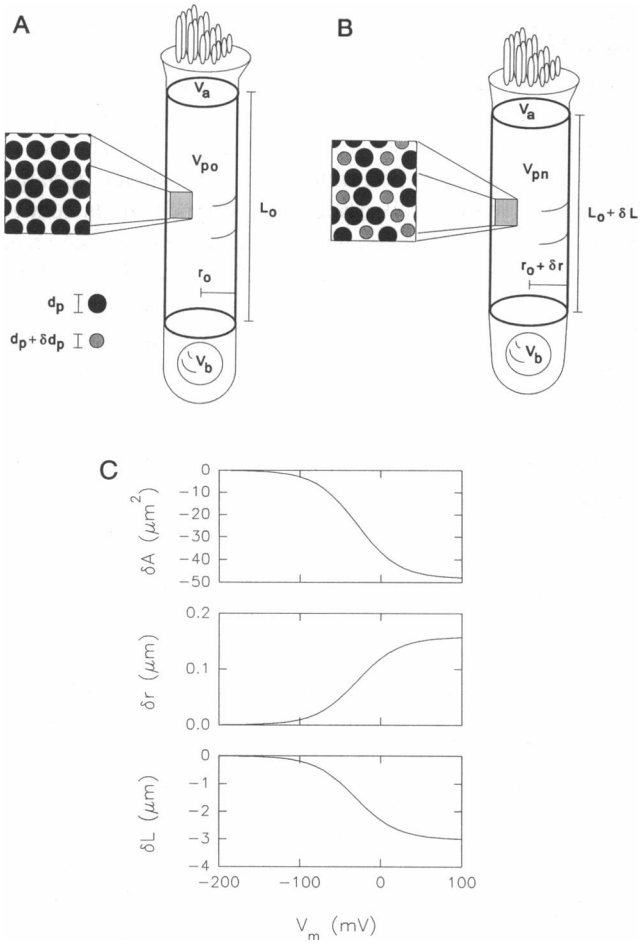

FIGURE 4 OHC mechanical model (see Results). (*A*) Hyperpolarized OHC in fully elongate state where all membrane particles (blow up) are in maximum surface area state. (*B*) Partially depolarized OHC where some particles are in minimum surface area state. Note that when cell is depolarized length is decreased and radius is increased. Drawing is not to scale. V_{p_o}, volume of portion of fully elongate cell which is bounded by active, particle containing region; r_o, radius of cell in fully elongate state; V_a, volume of apical region of cell not containing membrane particles; V_b, volume of basal region of cell not containing membrane particles; L_o, length of cell in fully elongate state; V_{p_n}, volume of portion of partially contracted cell which is bounded by active, particle containing region; δr, change in radius due to depolarization; δL, change in length of cell due to depolarization; d_p, particle diameter in maximum surface area state; δd_p, change in particle surface area in minimum surface area state. (*C*) Predicted change in model OHC surface area, radius, and length as a function of transmembrane voltage. Changes in length and radius are similar to experimental observations under voltage clamp. Ratio of length to radial change is about 18.

The maximum change in cell surface area (δA_{max}) depends upon the number of particles (N_t) in the membrane,

$$\delta A_{max} = \delta A_p N_t. \tag{7}$$

The aggregate membrane surface area change ($\delta A(V_m)$) will be voltage-dependent and will display the same Boltzmann characteristics of the voltage-dependent charge movement alluded to above (Santos-Sacchi, 1991).

$$\delta A(V_m) = \frac{\delta A_{max}}{1 + \exp((-ze/kT)\{V_m - V_h\})} \tag{8}$$

The architecture of an OHC is normally close to cylindrical, and the following analysis adheres to that form; however, since it is known that length changes occur even when the cell has swelled into a spherical form (Holley and Ashmore, 1988a), an analysis assuming the form of a prolate spheroid was performed and similar results were obtained. Forces need not be considered directly, but are simply acknowledged to promote the maintenance of the cylindrical shape (or, in the case of a spheroid model, the spheroid shape). The existence of a cytoskeletal spring beneath the OHC plasmalemma (Holley and Ashmore, 1988b), in conjunction with intracellular pressure is taken to provide these forces. The force providing the change in surface area derives from the imposed transmembrane voltage.

For the cylindrical cell model (Fig. 4), the volumes of the particle containing region of the cell before (V_{p_o}) and after (V_{p_n}) a change in length (δL) and radius (δr) are

$$V_{p_o} = \pi r_o^2 L_o, \tag{9}$$

and

$$V_{p_n} = \pi(r_o + \delta r)^2 (L_o + \delta L), \tag{10}$$

where L_o and r_o are the cell length and radius in the fully elongate state.

The total cell volumes before (V_o) and after (V_n) are

$$V_o = V_{p_o} + V_{ab}, \tag{11}$$

and

$$V_n = V_{p_n} + V_{ab}, \tag{12}$$

where V_{ab} is the sum of the volumes of the apical (V_a) and basal (V_b) regions of the cell which are devoid of the presumed membrane motor particles. To simplify matters, an assumption is made that V_{ab} remains constant. This assumption may be taken to indicate that the apical and basal compartments are either rigid or deformable to the extent that the sum of the volumes remains constant. Because total cell volume is constant for each condition,

$$\delta L = -\delta r L_o \frac{2r_o + \delta r}{r_o^2 + 2r_o\delta r + \delta r^2}. \tag{13}$$

The surface areas of the active, particle-containing regions under each condition are

$$A_o = 2\pi r_o L_o \tag{14}$$

$$A_n = 2\pi(r_o + \delta r)(L_o + \delta L), \tag{15}$$

The change in cell surface area, $\delta A(V_m)$, is then

$$\delta A(V_m) = A_n - A_o = \frac{\delta A_{max}}{1 + \exp\left(\frac{-ze}{kT}\{V_m - V_h\}\right)}. \tag{16}$$

Given the Boltzmann dependence of $\delta A(V_m)$, the cell volume constraint, and the further constraint that $|\delta r| < |r_o|$, physically realizable values of δL and δr are obtained. Fig. 4 *c* plots the solution to the equations as voltage is varied between −200 and 100 mV. The parameters used were: L_o, 50 μm; r_o, 5 μm; δd_p, −0.5 nm; and N_t, 4000/μm^2. The

number of particles derives not only from estimates based on the relation between charge movement and length changes in OHCs (Santos-Sacchi, 1991), but also from ultrastructural studies (Kalinec et al., 1992). The outcome of this model (Fig. 4 *c*) displays characteristics which are comparable to actual results obtained under whole cell voltage clamp (Ashmore, 1987; Santos-Sacchi and Dilger, 1988; Santos-Sacchi, 1989, 1991, 1992). For example, maximal length changes are about 20 times greater than radial changes, and while depolarization decreases cell length, cell radius is increased. More importantly for the present analysis, the model can be used to simulate the nonlinear effects evoked by sinusoidal voltage stimulation.

Fig. 5 illustrates the fundamental and harmonic structure of δL and V_m for the complete model (electrical and mechanical) when excited by those same frequencies used to collect the biophysical data. Several characteristics of the model output should be noted. First, it is obvious that phase relations are similar between model and data (Fig. 2). Second, the relative magnitudes of the fundamental and second harmonic mechanical responses resemble those of the actual mechanical data. Clearly, the relative magnitude of the second harmonic mechanical response is greater than would be predicted from the corresponding predicted voltage. Finally, note that while the magnitude of the voltage second harmonic increases with frequency, the magnitude of the mechanical second harmonic decreases with frequency. Overall, the model results are similar to the actual data in that they suggest that the second harmonic mechanical response is due to forces other than the second harmonic voltage.

Certainly, however, the voltage harmonics should induce mechanical responses at their respective frequencies. A model simulation was performed where the voltage from the nonlinear electrical cell model was stripped of its fundamental prior to evoking changes in membrane surface area. This was accomplished mathematically by zeroing the fundamental component of the voltage fast Fourier transform, followed by reverse transformation. Obviously, the fundamental component is absent in the mechanical response. Informatively, however, the voltage-dependent mechanical response at the second harmonic is unmasked. It mirrors the increase in magnitude which the second harmonic voltage displays. More importantly for this analysis, the phase of the mechanical response lags that of I_{R_s} by 3.14 rad, just as voltage does (Fig. 3).

It is shown in Fig. 6 that the fundamental component of the voltage, i.e., the voltage stripped of its harmonics (an ideal voltage clamp), induces a mechanical response which presents both fundamental and second harmonic structure. The magnitude of the second harmonic decreases with frequency less so than for the complete model (Fig. 5), and it appears to follow the similar slight decrease of the fundamental magnitude. The phase of the second harmonic relative to the current is somewhat similar to the complete model (Fig. 5), however, the phase lag is decreased at all frequencies. The apparent frequency dependence of the mechanical second harmonic phase is not real, but only reflects the frequency dependence of the I_{R_s} phase to which the mechanical

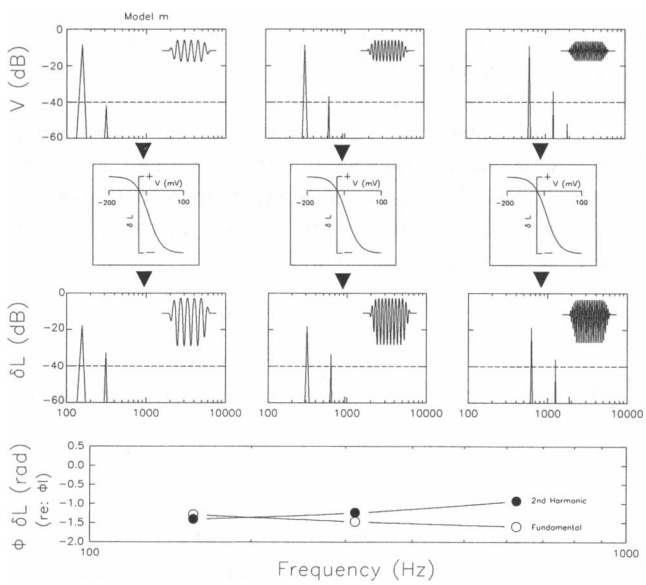

FIGURE 5 Combined electrical and mechanical model of OHC mechanical response under voltage clamp. Parameters as in Figs. 3 and 4. Upper panels depict the membrane voltage waveforms and magnitude responses obtained by FFT for the stimulus frequencies of 156, 313, and 625 Hz. Panels between arrowheads represent the V-δL function with parameters as in Results. Middle panels depict the mechanical waveforms and magnitude responses. Lower panel shows the phase of the mechanical response fundamental and second harmonic relative to the current phase. Phase is plotted versus fundamental frequency. Note that the mechanical second harmonic decreases with frequency unlike the voltage second harmonic. The phase response is similar to the actual biophysical data (Fig. 2).

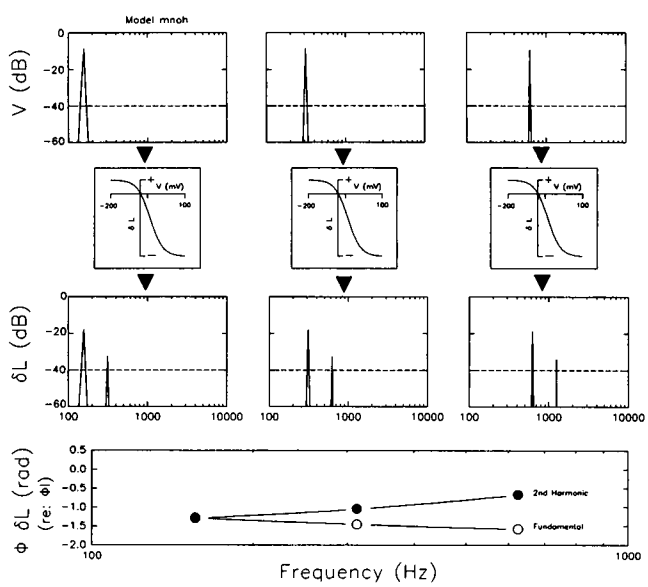

FIGURE 6 As in Fig. 5 except that the second harmonic voltage has been removed prior to generating the mechanical response. This is equivalent to an ideal voltage clamp, without the effects of series resistance. Note that mechanical second harmonics are generated due to the nonlinearity of the V-δL function. The phase is somewhat similar to the complete model (Fig. 5), but the second harmonic lag is slightly decreased at all frequencies (see Fig. 7).

phase is referenced. The phase of the mechanical second harmonic actually mirrors that of the fundamental, i.e., $\phi(\delta L_{fo}) = \phi(\delta L_{f1})/2$. The frequency independence of the mechanical second harmonic phase is demonstrated in Fig. 7, where the phase of the mechanical second harmonic of the fundamental-only model is plotted relative to that of the complete model (essentially, the phase reference to current is removed). Note, however, that a slight residual frequency dependence in this phase plot is revealed, showing a lag accumulating with frequency. This is totally attributable to the mechanical effects of the frequency-dependent increase in the magnitude of the voltage second harmonic of the complete model, given its phase lag of 3.14 rad. That is, in the complete model, and presumably in the actual data, although the second harmonic mechanical response is dominated by distortion in the mechanical transformation, voltage distortion plays a minor role.

DISCUSSION

In the present report, the higher harmonic components of the OHC voltage-dependent mechanical response were measured, and deduced through modeling to arise primarily from nonlinearities in the *V*-δL process. Voltage nonlinearities generated due to the OHC nonlinear capacitance (see Footnote 1), under nonideal voltage clamp, account for little of the mechanical harmonic distortion. Thus, while mechanical distortion can be induced by nonlinearities in the voltages of the OHC, the nonlinear nature of the mechanical transformation ensures distortion product generation under the present experimental conditions.

Effects of the *V*-δL function on evoked mechanical nonlinearities of the OHC

The form of the OHC *V*-δL function under voltage clamp can be fit by a two-state Boltzmann relation (Santos-Sacchi, 1991, 1992) and consequently the mechanical sensitivity of the cell, the slope of the *V*-δL function, varies depending upon resting potential. Because the normal resting potential lies at the hyperpolarizing saturation knee of the *V*-δL function, sinusoidal voltage excitation elicits both DC and harmonic mechanical distortion. The production of DC mechanical components has been documented (Santos-Sacchi, 1989; Evans et al., 1989), and the polarity of this component has been shown to reverse, as expected, when the holding potential is shifted to values more positive than V_h (the voltage (~−30 mV) at half-maximal length change (Santos-Sacchi, 1989, 1992)). Indeed, under voltage clamp, the DC component has been measured at stimulus frequencies as high as 3.2 kHz (Santos-Sacchi, 1992). Nevertheless, it was shown that the magnitude of the DC component is highly level-dependent, decreasing in size much more precipitously than the fundamental component as voltage level decreases (see Figs. 5 *c* and 10 *d* in Santos-Sacchi (1992)). This is a consequence of the inherent linearization of the *V*-δL function as stimulus amplitude is decreased. Modeling indicates that the same level dependence characterizes the mechanical harmonic components as well. In the intact, normal organ of Corti, these level-dependent effects will be expressed as auditory threshold is approached; that is, near auditory threshold, mechanically generated distortion will be several orders of magnitude smaller than the fundamental component, given a pure sinusoidal voltage stimulus.

In addition to level-dependent effects, mechanisms which alter the relationship between resting potential (operating point along the *V*-δL function) and V_h of the *V*-δL function will also influence the generation of nonlinearities. That is, shifts in either resting potential or V_h will modify the characteristics of mechanical distortion. For a two state Boltzmann process (namely, the *V*-δL function) which is symmetrical about its midpoint, V_h, the DC mechanical component theoretically will be abolished by superposition of the resting potential and V_h. Nonetheless, harmonic distortion will remain, and under these conditions predominantly odd harmonics will be generated. In the absence of superposition, level-dependent DC, odd and even harmonics are always expected. In the present study, harmonics above the second were probably below the noise floor.

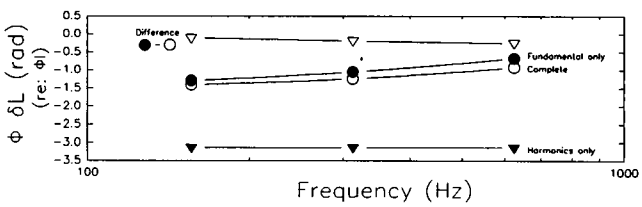

FIGURE 7 Relations between second harmonic mechanical phase data for the three model conditions: complete (fundamental and harmonic voltages, *open circles*), fundamental voltage only (*closed circles*), and harmonic voltage only (*closed triangles*). The difference between fundamental only and complete model (*open triangles*) essentially removes the reference to current and demonstrates the minimal frequency dependence of the mechanical phase. The remaining slight frequency dependence (increasing lag with frequency) is due to the effects of the mechanical response induced by second harmonic voltage, since this voltage driven response increases in magnitude with frequency, and has a phase lag of −3.12 rad.

Modeling the mechanism of OHC motility

The similarity between characteristics of OHC nonlinear charge movement (indicative of membrane-bound voltage sensors) and OHC motility has been suggested to indicate that an estimated 4000/μm^2 membrane-bound voltage sensor-motor elements control OHC length (Santos-Sacchi, 1991, 1992). In the present report, the mechanism responsible for OHC motility was modeled as a modification of membrane surface area due to a two state voltage-dependent conformational change of an intrinsic membrane particle, representing the sensor-motor element. Intrinsic membrane particles, presumably membrane proteins, have been observed in the OHC lateral plasmalemma (Gulley and Reese, 1977; Saito, 1983; Forge, 1991; Kalinec et al., 1992). The density of particles is similar to estimates based on nonlinear charge data.

Kalinec et al. (1992) have provided evidence that voltage-dependent OHC length changes continue to occur after subplasmalemmal cytoskeletal elements are disrupted with intracellular trypsin. In fact, they report that membrane patches change surface area when hyperpolarized or depolarized—hyperpolarization increases the membrane patch area, while depolarization decreases it. They have suggested that a rearrangement of membrane particles within the plasmalemma induces a change in membrane surface area, and a concomitant change in OHC length. Furthermore, these same investigators (Kalinec et al., 1993) have speculated that tetrameric anion exchangers in the lateral OHC membrane underlie OHC motility. However, according to their model, it is not clear how two-state tetrameric rearrangements of the observed membrane particles within the OHC membrane can account for the one-to-one correspondence between voltage sensor and motor element derived from nonlinear charge movement and motility data (Santos-Sacchi, 1991, 1992; Ashmore, 1992); that is, the reduced number of discrete motor elements (four per element rather than one per element; hence, one quarter the density of membrane particles) might predict results contrary to experimental observations relating nonlinear charge movement and motility.

Dallos et al. (1991a) have presented a model of OHC motility based on a "motor unit" of circumferentially arranged discrete sensor-motor elements which acts in series along the length of the OHC. The model accurately predicts motility data obtained with the partitioning microchamber technique (Dallos et al., 1991b). The motor elements are predicted to be anisotropic, providing a greater displacement in the longitudinal direction than in the radial direction. The putative alignment of the individual motor's displacement vector (~20°) roughly corresponds to an early estimate of the angle of the circumferential filaments described by Holley and Ashmore (1988b). Newer estimates of the filament angle are closer to 9°, although the range is substantial (−55° to 74° (Holley et al., 1992)). It should be noted that recently Iwasa and Chadwick (1992) presented evidence that the active tension within the OHC plasma membrane is likely to be isotropic. Furthermore, they suggested that the presumed motors are not aligned within the plasmalemma.

The simple model developed in the present report is fundamentally isotropic, but evokes anisotropic shape changes in the OHC due to the geometric constraints of the cell architecture (see Results). The modifications in cell surface area are simply governed by changes in particle (protein) conformation and attendant reductions in the area of the particle within the lipid bilayer. The lipid bilayer is assumed to instantaneously occupy the potential void created by the particle's reduced area; the particle need not be spherical as depicted. It is the simplest model available to fit the whole-cell voltage-clamped OHC, and its usefulness is evident from the similarity between model predictions and data.

Voltage nonlinearities of the OHC

As was demonstrated through modeling, nonlinear voltages will evoke voltage-induced mechanical responses. The degree to which these voltage nonlinearities contribute to the measured mechanical nonlinearities will depend upon their magnitudes. Voltage nonlinearities will arise from several processes known to exist within distinct domains of the OHC plasmalemma. The very process that translates acoustically driven stereociliar movements into OHC receptor currents is nonlinear (Russell et al., 1986; Dallos, 1986). That is, opposite but equal displacements of the hair bundle from the resting position generate asymmetrical conductance changes, resulting in asymmetrical voltage responses. Whereas it is probable that the only channel in the apical membrane of hair cells is the stereociliary transduction channel, a variety of ionic channel types is found in the basolateral membrane, including voltage-dependent K^+, and Ca^{2+} channels (Santos-Sacchi and Dilger, 1988; Ashmore and Meech, 1986; Nakagawa et al., 1991; Housley and Ashmore, 1992), as well as ligand gated channels (e.g., Housley and Ashmore, 1991). In addition to these nonlinearities, there exists the unique motility-related voltage-dependent capacitance of the OHC (Ashmore, 1989; Santos-Sacchi, 1990, 1992; Iwasa, 1993). Thus, the intrinsically nonlinear receptor potential registered in the OHC cell may be further affected by the nonlinear RC properties of the basolateral membrane.

It would be useful to have an estimate of the contribution of these basolateral membrane nonlinearities to the mechanical response in the in vivo state. Because the membrane nonlinearities which can potentially affect OHC motility on a cycle-by-cycle basis[2] are voltage and time-dependent, hence stimulus level and frequency-dependent, it is possible to rule out specific contributions based on stimulus parameters. That is, considering stimulus frequencies above 200 Hz and sound pressure levels below that required to generate 5-mV Pk AC receptor potentials,[3] certain basolateral characteristics can be ignored. This is not an unreasonable approach, since the feedback effects of OHC motility are presumed to be most important at low stimulus magnitudes, where tuning is greatest. In order to evaluate whether a basolateral membrane characteristic can be ignored given these stimulus constraints, the time- and voltage-dependent nature of that characteristic must be considered. It becomes readily apparent, then, that the contribution of many of the basolateral conductances can be ignored in a model analysis at the typical in vivo resting potential of −70 mV (Dallos et al. (1982); see Footnote 3 in Santos-Sacchi (1989)). For example, the outward K^+ conductance, which dominates the basolateral membrane conductance, can be ignored because the activation time constant is on the order of tens of milliseconds at potentials near its activation voltage of about −50 mV (Santos-Sacchi and Dilger, 1988; Housley and Ashmore, 1992). The same rea-

[2] Ligand gated channels typically are slower in their action than voltage or mechanically gated channels, and may be considered to have mainly steady state effects on membrane potential and or V_h. For example, the effects of efferent transmitters on the OHC may produce hyperpolarization (Housley and Ashmore, 1991) or shifts of V_h (Huang and Santos-Sacchi, 1993).

[3] A 5-mV Pk response from the OHC is obtained with moderate intensities at the cell's characteristic frequency (Dallos, Santos-Sacchi and Flock, 1982).

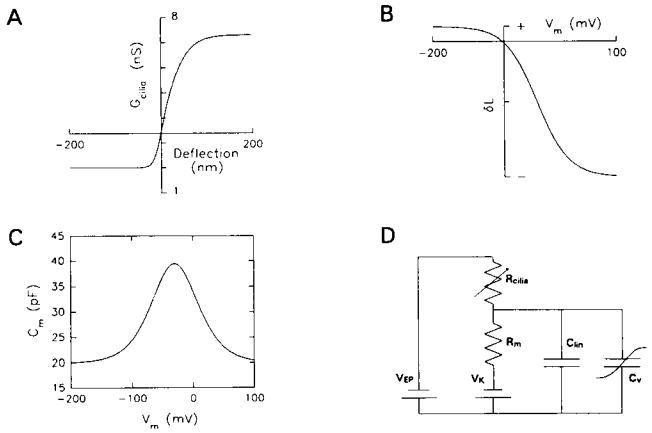

FIGURE 8 Nonlinearities of the in vivo model. (*A*) Conductance of the apical membrane of the OHC, including transducer conductance (max 5.3 nS) and leakage conductance (2 nS). The form is that observed by Kros et al. (1992). However, the resting conductance is shifted to the right so that about 25% of the transducer conductance is active. Under these conditions the model generates voltage responses which are similar to those obtained in OHCs from the 3rd turn of the guinea pig cochlea (Dallos, 1986). (*B*) *V*-δ*L* function with parameters as in Results. (*C*) Voltage-dependent capacitance function with parameters as in Results. (*D*) In vivo electrical model. R_{cilia}, resistance of apical OHC membrane whose conductance is depicted in *A*; R_m, basolateral membrane resistance of 40 MΩ; V_{ep}, endolymphatic potential of +90 mV; V_k, potassium reversal potential of −90 mV; C_{lin}, linear membrane capacitance of 20 pF; C_v, voltage-dependent membrane capacitance depicted in *C*. Stimulation of the model is via transducer conductance changes induced by sinusoidal deflection of the strereociliar bundle as in *A*. Resting potential under these conditions is near −67 mV.

soning holds for the basolateral Ca^{2+} conductance (Santos-Sacchi and Dilger, 1988; Nakagawa et al., 1991). While it is known that a nonlinear leakage conductance remains even after considerable attempts to block the OHC voltage-dependent conductances (Santos-Sacchi, 1991; Huang and Santos-Sacchi, 1993), the slope conductance near resting potential is fairly linear. In fact, Housley and Ashmore (1992), have shown that even with "normal" intra- and extracellular solutions the slope conductance between −50 and −85 mV is nearly constant for a given cell under voltage clamp, although it varies as a function of cell length. Thus, with the given stimulus parameter constraints, it seems acceptable to model the OHC as an electromechanical system comprised of only three nonlinearities—the transducer conductance, the voltage-dependent capacitance, and the *V*-δ*L* function.

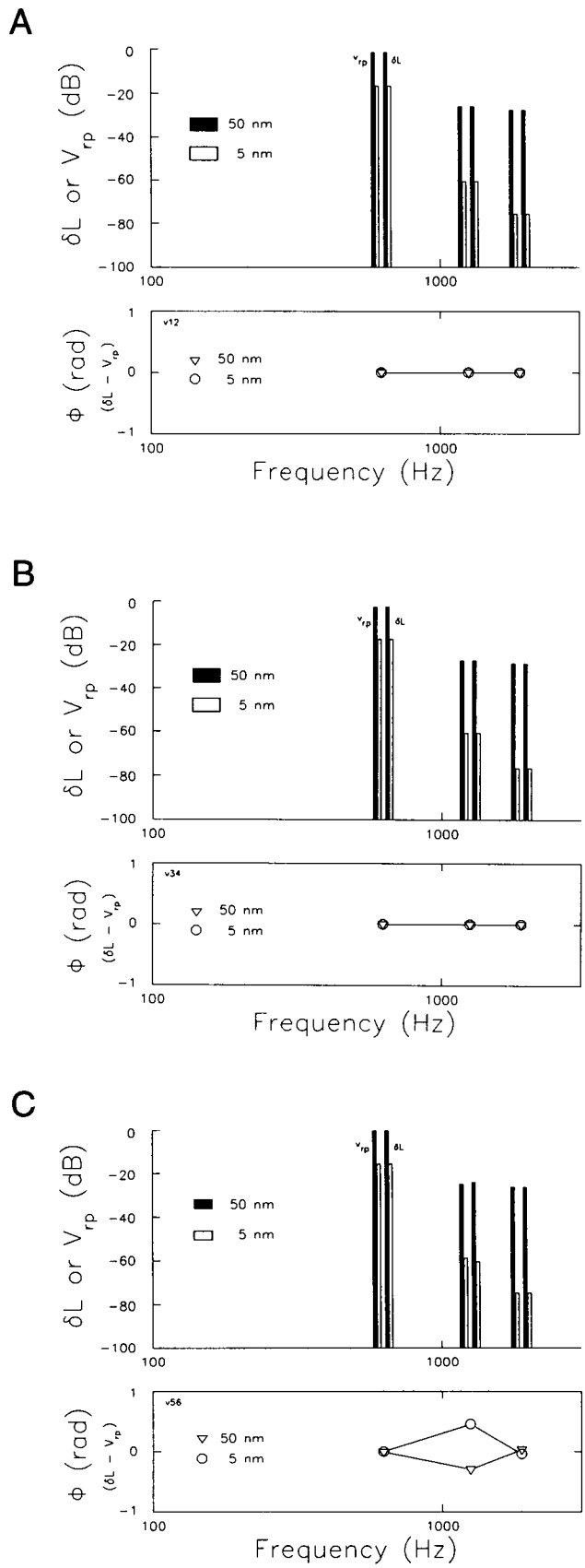

FIGURE 9 (*A*) Magnitudes and phases of receptor potentials (V_{rp}) and mechanical responses (δ*L*) generated by sinusoidal stereociliar deflections of 5- and 50-nm Pk in the in vivo model with only the transducer nonlinearity. A fixed membrane capacitance of 30 pF and a linear *V*-δ*L* function were employed. Note the generation of fundamental, second, and third harmonics in the voltage and consequently in the mechanical response. Magnitudes (responses were scaled to set fundamentals equal) and phases are the same for voltage and mechanical response. (*B*) As above, except that the nonlinear capacitance has been introduced. At the voltages generated, little or no effect of the nonlinear capacitance is observed. (*C*) As above, except that the nonlinear *V*-δ*L* function is added. Only slight changes in the magnitudes and phases of the harmonics are evident, indicating that the dominant nonlinearity which influences distortion in the mechanical response is due to the transducer function.

The forms of these nonlinearities and the in vivo electrical model are displayed in Fig. 8. The form of the transducer conductance of the OHC is that determined by Kros et al. (1992). However, the resting point has been shifted to the right to correspond more closely with in vivo measures (Fig. 8 in Dallos (1986)). Fig. 9 *a* presents a comparison between receptor potential (at 625 Hz) and induced mechanical responses when the voltage-dependent capacitance and V-δL function are linearized. It is clear that harmonic distortion (evident as a second and third harmonic) is present in the receptor potential, and that mechanical response distortion simply mirrors this voltage distortion. In Fig. 9 *b*, the nonlinear capacitance is introduced. At the magnitudes of the receptor potential generated by the 50- and 5-nm Pk stereociliar displacements (~7 and ~1 mV peak-to-peak, respectively), the voltage-dependent capacitance induces minimal additional distortion in the voltages and mechanical responses (compare Figs. 9 *a* and 9 *b*). Finally, when the the nonlinear V-δL function is added (Fig. 9 *c*), it is observed that the mechanical response displays only slight differences in the magnitudes and phases of the mechanical response harmonics viz a viz the voltage. It is clear from this modeling effort that the dominant factor contributing to distortion production in the mechanical response in vivo will be the transduction process nonlinearity.

Patuzzi et al. (1989) have previously argued that the transducer mechanism nonlinearity of the OHC dominates in the in vivo cochlea. While this is in accord with the present modeling effort, it cannot be dismissed that the magnitude and/or effectiveness of the mechanical nonlinearity may be different in vivo. For example, it is clear that the position of the V-δL function is not static—it can be shifted along the voltage axis (Santos-Sacchi, 1991; Huang and Santos-Sacchi, 1993; Evans et al., 1991). That is, the operating point can be placed in a more or less linear portion of the function. Clearly, in vivo estimates of this nonlinearity are necessary.

SUMMARY

The voltage-induced mechanical properties are believed to provide the means whereby the auditory system enhances its frequency sensitivity and selectivity (Dallos, 1992). Nonlinearity in the peripheral auditory system is believed to be the hallmark of the enhancement mechanism. It is demonstrated here that under voltage clamp, OHC mechanical responses possess nonlinear attributes. The mechanical harmonic components observed are effected by the nonlinear nature of the V-δL function, since through modeling it is shown that the voltage harmonic distortion generated under nonideal voltage clamp of the OHC contributes minimally. While these conclusions hold for the data obtained with large voltage clamp stimuli, modeling efforts indicate that in vivo, at moderate sound pressure levels and below, the dominant factor which contributes to nonlinearities of the OHC mechanical response resides within the process that translates stereociliar movement into receptor potentials.

This work was supported by an National Institute of Deafness and other Communication Disorders Research Career Development Award and National Institutes of Health grant DC00273.

REFERENCES

Ashmore, J. F., and R. W. Meech. 1986. Ionic basis of the resting potential in outer hair cells isolated from the guinea pig cochlea. *Nature (Lond.).* 322:368–371.

Ashmore, J. F. 1987. A fast motile response in guinea-pig outer hair cells: the cellular basis of the cochlear amplifier. *J Physiol (Lond.).* 388: 323–347.

Ashmore, J. F. 1989. Transducer motor coupling in cochlear outer hair cells. *In* Mechanics of Hearing. D. Kemp and J. P. Wilson, editors. Plenum Press, New York. 107–113.

Ashmore, J. F. 1992. Mammalian hearing and the cellular mechanisms of the cochlear amplifier. *In* Sensory Transduction. D. P. Corey, and S. D. Roper, editors. Rockefeller University Press, New York.

Brownell, W. E. 1992. Outer hair cell electromotility and otoacoustic emissions. *Ear Hear.* 11:82–92.

Dallos, P., J. Santos-Sacchi, and Å. Flock. 1982. Intracellular recordings from outer hair cells. *Science (Wash. DC).* 218:582:584.

Dallos, P. 1986. Neurobiology of cochlear inner and outer hair cells: intracellular recordings. *Hear. Res.* 22:185–198

Dallos, P., R. Hallworth, and B. N. Evans. 1991a. Stochastic theory of outer hair cell electromotility. *In* Auditory Physiology and Perception. Y. Cazals, K. Horner, and L. Demany, editors. Pergamen Press, Oxford, England. 35–43.

Dallos P, B. N. Evans, and R. Hallworth. 1991b. On the nature of the motor element in cochlear outer hair cells. *Nature (Lond.).* 350:155–157.

Dallos, P. 1992. The active cochlea. *J. Neurosci.* 12:4575–4585.

Evans, B. N., P. Dallos, and R. Hallworth. 1989. Asymmetries in motile responses of outer hair cells in simulated in vivo conditions. *In* Mechanics of Hearing. D. Kemp, and J. P. Wilson, editors. Plenum Press, New York. 205–206.

Evans, B. N., R. Hallworth, and P. Dallos. 1991. Outer hair cell electromotility: the sensitivity and vulnerability of the DC component. *Hear. Res.* 52:288–304.

Forge, A. 1991. Structural features of the lateral walls in mammalian cochlear outer hair cells. *Cell Tissue Res.* 265:473–483.

Gulley, R. L., and T. S. Reese. 1977. Regional specialization of the hair cell plasmalemma in the organ of Corti. *Anat. Rec.* 189:109–124

Holley, M. C., and J. F. Ashmore. 1988a. On the mechanism of a high-frequency force generator in outer hair cells isolated from the guinea pig cochlea. *Proc. R. Soc. Lond. Ser. B Biol. Sci.* 232:413–429.

Holley, M. C., and J. F. Ashmore. 1988b. A cytoskeletal spring in cochlear outer hair cells. *Nature (Lond.).* 335:635–637.

Holley, M. C., F. Kalinec, and B. Kachar. 1992. Structure of the cortical cytoskeleton in mammalian outer hair cells. *J. Cell Sci.* 102: 569–580.

Housley, G. D., and J. F. Ashmore. 1991. Direct measurement of the action of acetylcholine in outer hair cells of the guinea pig cochlea. *Proc. R. Soc. Lond. Ser. B Biol. Sci.* 244:161–267.

Housley, G. D., and J. F. Ashmore. 1992. Ionic currents of outer hair cells isolated from the guinea-pig cochlea. *J. Physiol. (Lond.).* 448: 73–98.

Huang, G.-J., and J. Santos-Sacchi. Metabolic control of OHC function: phosphorylation and dephosphorylation agents shift the voltage dependency of motility related capacitance. Midwinter meeting of the Association for Research in Otolaryngology, St. Petersburg, FL, February 1993.

Iwasa, K. H., and R. S. Chadwick. 1992. Elasticity and active force generation of cochlear outer hair cells. *J. Acoust. Soc. Am.* 6:3169–73.

Iwasa, K. H. 1993. Effect of stress on the membrane capacitance of the auditory outer hair cell. *Biophysical J.* 65:492–498.

Kalinec, F., M. C. Holley, K. H. Iwasa, D. J. Lim, and B. Kachar. 1992. A membrane-based force generation mechanism in auditory sensory cells. *J. Proc. Natl. Acad. Sci. USA.* 89:8671–8675.

Kalinec, F., R. A. Urrutia, R. G. Jaeger, D. J. Lim, and B. Kachar. Membrane channel proteins and the force generator mechanism in the lateral wall of

cochlear outer hair cells. Midwinter meeting of the Association for Research in Otolaryngology, St. Petersburg, FL, February, 1993.

Kros, C. J., A. Rusch, and G. P. Richardson. 1992. Mechano-electrical transducer currents in hair cells of the cultured neonatal mouse cochlea. *Proc. R. Soc. Lond. Ser. B Biol. Sci.* 249:185–193.

Nakagawa, T., S. Kakehata, N. Akaike, S. Komune, T. Takasaka, and T. Uemura. 1991. Calcium channel in isolated outer hair cells of guinea pig cochlea. *Neurosci. Lett.* 125:81–84.

Patuzzi, R. B., G. K. Yates, and B. M. Johnstone. 1989. Outer hair cell receptor current and sensorineural hearing loss. *Hear. Res.* 42:47–72.

Ruggero, M. A. 1992. Responses to sound of the basilar membrane of the mammalian cochlea. *Curr. Opin. Neurobiol.* 2:449–456.

Russell, I. J., A. R. Cody, and G. P. Richardson. 1986. The responses of inner and outer hair cells in the basal turn of the guinea-pig cochlea and in the mouse cochlea grown in vitro. *Hear. Res.* 22:199–216

Saito, K. 1983. Fine structure of the sensory epithelium of guinea pig organ of Corti: subsurface cisternae and lamellar bodies in the outer hair cells. *Cell Tissue Res.* 229:467–481.

Santos-Sacchi, J., and J. P. Dilger. 1988. Whole cell currents and mechanical responses of isolated outer hair cells. *Hear. Res.* 35:143–150.

Santos-Sacchi, J. 1989. Asymmetry in voltage dependent movements of isolated outer hair cells from the organ of Corti. *J. Neurosci.* 9:2954–2962.

Santos-Sacchi, J. 1990. Fast outer hair cell motility: how fast is fast? *In* The Mechanics and Biophysics of Hearing. P. Dallos, C. D. Geisler, J. W. Matthews, M. A. Ruggero, and C. R. Steele, editors. Springer-Verlag, Berlin. 69–75.

Santos-Sacchi, J. 1991. Reversible inhibition of voltage-dependent outer hair cell motility and capacitance. *J. Neurosci.* 11:3096–3110.

Santos-Sacchi, J. 1992. On the frequency limit and phase of outer hair cell motility: effects of the membrane filter. *J. Neurosci.* 12:1906–1916.